Flexible and Printed Electronics

Anode ink formulation for a fully printed flexible fuel cell stack

IOP Publishing Flex. Print. Electron. 5 (2020) 025002 https://doi.org/10.1088/2058-8585/ab7e16

Flexible and Printed Electronics

PAPER

Anode ink formulation for a fully printed flexible fuel cell stack

Liisa Hakola[1], Andres Parra Puerto[2], Anu Vaari[1], Tiina Maaninen[1], Anthony Kucernak[2], Saara Viik[1] and Maria Smolander[1]

[1] VTT Technical Research Centre of Finland Ltd., Espoo, Finland
[2] Imperial College London, SW7 2AZ, United Kingdom

E-mail: liisa.hakola@vtt.fi

Keywords: fuel cell, anode, stack, catalyst, print, inkjet, ink, formulation, flexible

OPEN ACCESS

RECEIVED
4 September 2019

REVISED
24 February 2020

ACCEPTED FOR PUBLICATION
9 March 2020

PUBLISHED
20 April 2020

Abstract

In fuel cells the underlying reactions take place at the catalyst layers composed of materials favoring the desired electrochemical reactions. This paper introduces a formulation process for a catalyst inkjet ink used as an anode for a fully printed flexible fuel cell stack. The optimal ink formulation was 2.5 wt% of carbon–platinum–ruthenium mixture with 0.5% Nafion concentration in a diacetone alcohol solvent vehicle. The best jetting performance was achieved when 1 wt% binder was included in the ink formulation. Anodes with resistivity of approximately 0.1 Ω cm were inkjet printed, which is close to the commercial anode resistivity of 0.05 Ω cm. The anodes were used in fuel cell stacks that were prepared by utilizing only printing methods. The best five-cell-air-breathing stack showed an open circuit potential under H_2/air conditions of 3.4 V. The peak power of this stack was 120 μW cm^{-2} at 1.75 V, with a resistance obtained from potentiostatic impedance analysis of 295 Ohm cm^2. The printed electrodes showed a performance suitable for low-performance solutions, such as powering single-use sensors.

1. Introduction

Printing processes are potential methods for fabricating electronic devices, including electrochemical devices, such as fuel cells. Printing processes can be used to print many of the layers of a fuel cell device, such as electrodes or current collectors. Since the manufacture of electrochemical devices requires accuracy, reliability and reproducibility at low cost [1], printing processes are considered suitable candidates for all fabrication steps [2]. Printing processes make it possible to realize flexible versions of fuel cells, thus enabling new types of applications and integration into flexible devices (e.g. wearables), or packaging the power source where space is tight.

Lesch *et al* have, in their recent review, evaluated the suitability of inkjet printing as a fabrication method for electrochemical devices, such as fuel cells [1]. An inkjet is a non-contact digital printing method widely used in commercial, desktop, packaging and industrial printing onto a wide range of substrates. Inkjet printing also has many applications in the manufacture of printed electronics, optics and opto-electronic devices. Inkjet technologies can be divided into continuous stream (CS) and drop-on-demand (DOD) inkjet. These technologies are further broken into sub-technologies that differ from each other in their drop formation or directing mechanisms. Piezoelectric DOD is the most common inkjet technology for printing functional materials, because drop formation is based on deformation of a piezoceramic element instead of the heat present in thermal DOD, and there is no ink recirculation, such as in CS. In inkjet printing, liquid ink droplets are sprayed from tiny nozzles directly onto the substrate according to the digital page data. The nozzle arrays are located in printheads as stationary page-wide elements, which increases the reliability and accuracy of the process control and the printing speed. As the ink droplets strike the substrate, they spread out immediately, depending on their kinetic energy and the surface tension of the ink. After spreading, the ink solvent starts to evaporate, and the ink can also absorb and penetrate into the substrate [3, 4].

Printing-based manufacturing processes are very interesting techniques for mass production of fuel cell technologies due to the cost reduction and the possibility of a one step process involving low-temperature polymer electrolyte fuel cells (PEMFC) due to the layered structure and compatible materials. In H_2-PEMFCs, H_2 is used as fuel due to the very fast reaction kinetics of the H_2 [5, 6] and the lower requirement for precious group metal (PGM) catalysts. Electrochemical conversion devices, such as fuel

cells, convert the chemical energy of a fuel by electrochemical oxidation and reduction into electricity. These devices have become more attractive in recent years due to the need to shift from oil, coal and natural gases to renewable energy sources [7]. In fuel cells the underlying reactions take place at the catalyst layers composed of materials favoring the desired electrochemical reactions [1].

The core of the PEMFC device is called the membrane electrode assembly (MEA) [8]. This MEA has three parts: two catalyst layers acting as an anode (oxidation reaction, H_2) and cathode (reduction reaction, O_2) and a proton-conducting ionomer membrane, which allows proton conductivity, but is electrically isolated between the anode and the cathode. Nafion® is the most commonly used membrane [9]. This MEA is assembled with a gas diffusion layer (GDL) for each electrode side, which is typically carbon paper with a grade of hydrophobicity that improves the mass transport of the reactants to the catalyst layer and helps the water removal to avoid flooding of the catalyst layer. Current collectors assist in the current collection produced in the electrochemical reaction and connect the fuel cell to external loads, and can have a flow field pattered for the gas or liquid flow.

An alternative fuel to hydrogen, which can be used within PEMFCs, is methanol, which can be made from renewable sources. Methanol has a higher energy density than hydrogen [10, 11] and offers some benefits as it is easier to handle and transport (liquid under normal conditions). Fuel cells utilizing methanol as fuel are usually known as direct methanol fuel cells (DMFCs). Methanol is seen as an interesting alternative for the current metal-based batteries, specifically in portable electronics [12, 13]. There the issues with shorter lifetime and higher cost per W, typical of current state-of-the-art DMFCs, are not necessarily limiting factors compared to existing battery solutions [14, 15]. The major difference with the H_2-PEMFC is the anode catalyst loading (much higher in DMFCs) and composition (PtRu-alloy in the DMFC instead of Pt) to improve the catalytic activity towards the methanol oxidation reaction [16, 17].

In H_2-PEMFC and DMFC, hydrogen and methanol are oxidized catalytically at the anode producing electrons and protons. The protons migrate through a proton exchange membrane and react catalytically with oxygen to produce water that is consumed at the anode. The electrons are transported through an external circuit from the anode to the cathode, thus providing power to connected devices. In the H_2-PEMFC, hydrogen is adsorbed in the Pt surface and fully oxidized into protons. In a DMFC, methanol and water are adsorbed on a catalyst surface, usually Pt particles, and lose protons until carbon dioxide is formed. If pure Pt is used as the catalyst in a DMFC, the oxidation reaction might not be complete because of the formation and subsequent irreversible absorption of CO and CHO intermediate species, which severely impede the kinetics of methanol oxidation on Pt [14, 15]. To mitigate the effect of these formed, often poisonous, species, the Pt catalyst is usually alloyed with second metals, such as Ru, Sn, Mo, Co or Ni. Combinations of Pt and Ru as the catalyst exhibit the highest reaction activity, power density and stability. To bring down the material costs and to increase mass activity, PtRu particles are typically supported on a high surface area carbon powder [14, 18].

Since the catalyst costs can represent up to 24% of the total system costs [7], it is worth considering how to use the catalyst in the most efficient way and not to waste it during the manufacturing process. As an additive printing method, the inkjet printing method offers precise microscale patterning, uniformity of deposited layers, thin layer deposition suitable for low catalyst loading, material grading, scalability and a low level of material waste during manufacturing [1, 7]. These advantages make inkjet printing suitable for printing expensive materials, such as PtRu particles. The printed anode contains both proton- and electron-conducting materials, and a catalyst, and can be used as a part of MEA, combining both anode and cathode functionalities (figure 1).

Typically, the most critical manufacturing steps in the fuel cell manufacturing process are catalyst loading and MEA fabrication [15]. This paper focuses on delivering a solution for a high performance anode to be used as a part of a fully printed flexible fuel cell stack. The stack design is very convenient because it can easily be use- with either H_2 or methanol as fuels, in an air-breathing (or fully passive) mode which relies on natural convection to provide oxygen. The main goal is to develop a stable ink formulation that is inkjet printable with both laboratory-scale and industrial-scale printheads. An inkjet printed anode is developed and characterized from printability and performance aspects in this paper, and finally used as an electrode for a fully printed fuel cell stack that is thin and flexible.

2. Materials and methods

The anode ink formulation consisted of the catalyst, Nafion and solvent. A commercial mixture of carbon black (C), Pt and Ru was used as the catalyst (Pt 40 wt%, Ru 20 wt% on Vulcan) from Quintech (C-Pt/Ru). The Nafion solution was from Sigma-Aldrich, and it contained 5 wt% Nafion perfluorinated resin solution in lower aliphatic alcohols and 15%–20% water (Nafion solution). Diacetone alcohol (DAA) was used as the main solvent in the inkjet ink formulation. Polyvinyl pyrrolidone (PVP) with ~10 000 molecular weight (mW) or Hypemer KD-14 (KD-14) from Croda Nordica was used as a binder.

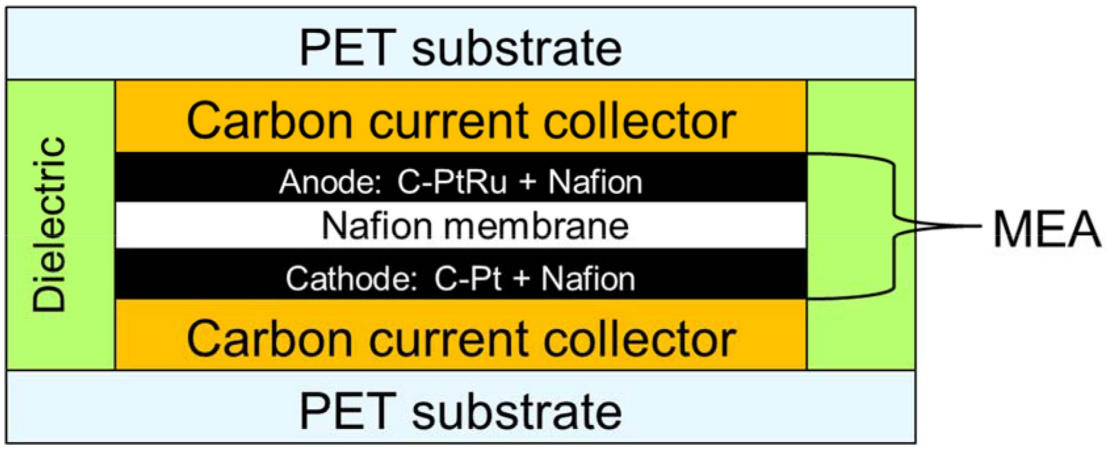

Figure 1. Layers for a printed one-cell fuel cell device.

The cathode material was a commercial mixture of carbon black and Pt (Pt 40 wt% on Vulcan) from Quintech (C-Pt). KD-14 was used as a binder.

Carbon-based ink from Dycotech Materials Ltd (CM-CAP-4311S) was used for screen printing the current collectors. Dielectric ink from Henkel Electrodag (PF-455B) and a glue layer from Dycotech Materials Ltd (DM-ADH-11001S) were used for screen printing the dielectric layer around the current collectors and for lamination, respectively.

The substrates used were photographic paper (Intelicoat Technologies) and PET (PolyEthylene Terephthalate) substrate with 125 μm thickness.

For anode ink characterization surface tension and viscosity were measured. Surface tension was measured with Aqua Pi Instrument from Kibron Inc. Viscosity was measured with Anton Paar MCR-301 rheometer at +20 °C.

For analysis of the particle size of the inks, a particle size analyzer (PAMAS S4031, PAMAS GmbH) with a sensor (HCB-LD-25/25) was used.

Two inkjet printers were used for printing the anodes: (1) a laboratory scale multinozzle inkjet printer based on single use printhead cartridges (DMP-2850, Fujifilm Dimatix) with 10 pl drop size (laboratory-scale printheads), and (2) a laboratory scale multinozzle printer (PiXDRO LP50, Meyer Burger) with industrial printheads (SL-128, Fujifilm Dimatix) with 80 pl drop size (industrial printheads). Cathodes and pure Nafion were inkjet printed with the first printer. Sheet-fed screen printing was used for printing the current collector, dielectric and glue.

Holes through the PET substrate and current collectors were made using a UV laser. Afterwards the holes were temporarily blocked by screen printing a sacrificial layer of carboxy methyl cellulose (CMC) at the reverse side of the substrate. Blocking is required in order to be able to print the anodes and cathodes without the electrode inks going through the holes. The water-soluble CMC can be washed off when adding the analyte and/or fuel. The process is described in detail in figure 2.

The printed layer thickness was measured with a Veeco Dektak 150, and the same instrument was used to acquire the thicknesses of profile images. The measurement distance for each of the 10 parallel thickness measurements was 811 μm.

Resistivity was determined by measuring the voltage with two instruments both based on a four-point probe measurement (principle in figure 3). The van der Pauw resistivity was measured with a Keithley 4200-SCS multimeter [19] and linear resistivity with an Agilent 34411A digit multimeter. The van der Pauw method is suitable for measuring the properties of a sample of any arbitrary shape. This method employs a four-point probe placed around the perimeter of the sample. This allows the van der Pauw method to provide an average resistivity of the sample, whereas a linear array provides the resistivity in the sensing direction.

The van der Pauw resistivity ρ_{avg} can be derived from a total of eight measurements made around the periphery of the sample with the configuration in figure 4, and can be calculated from the formula:

$$\rho_{\mathrm{avg}} = \frac{\rho_A + \rho_B}{2} = \frac{\frac{\pi}{\ln 2} f_A t_s \frac{(V_1 - V_2 + V_3 - V_4)}{4I} + \frac{\pi}{\ln 2} f_B t_s \frac{(V_5 - V_6 + V_7 - V_8)}{4I}}{2}$$

where

ρ_A and ρ_B are volume resitivities (Ω cm),
t_s is the thickness of the sample (cm),
V_1–V_8 are the voltages measured (V),
I is the current through the sample (A) and
f_A and f_B are geometrical factors based on sample symmetry; here they are 1, because the probes are aligned in perfect symmetry.

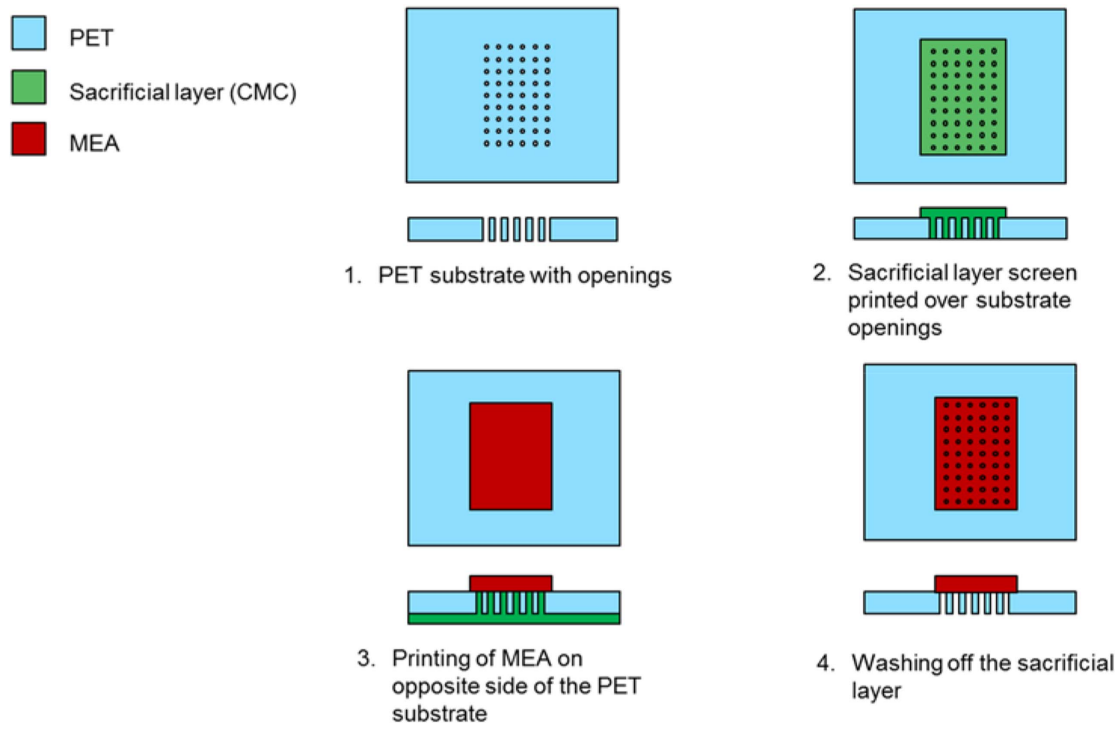

Figure 2. The process for blocking the holes on the current collector.

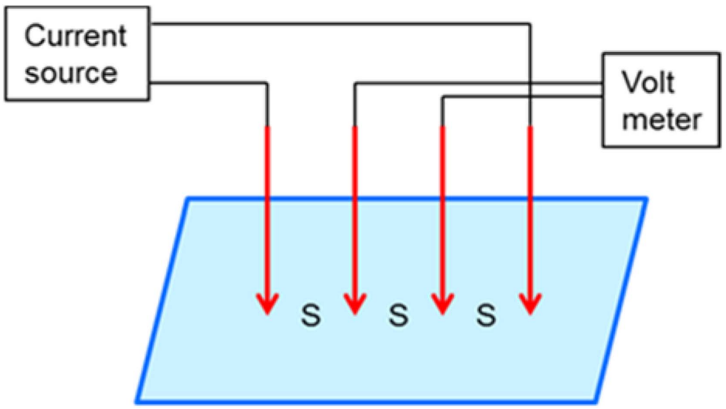

Figure 3. The principle of four-point probe measurement for sheet resistance. S is the needle spacing.

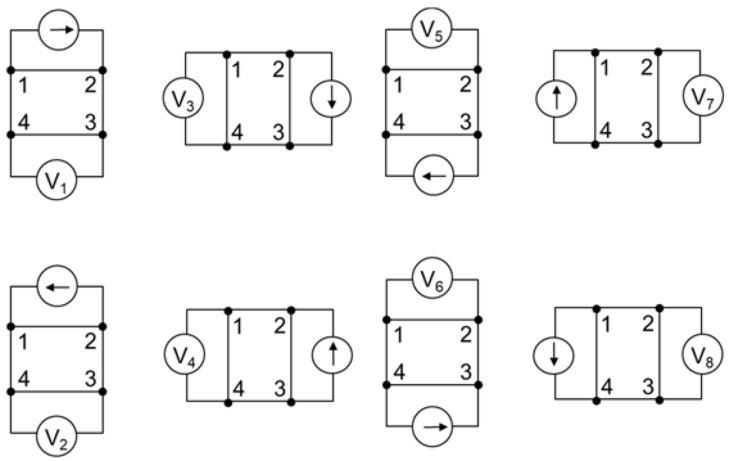

Figure 4. The van der Pauw resistivity configurations [19].

Linear resistivity ρ can be calculated from the formula:

$$\rho = \frac{\pi}{\ln 2} t \left(\frac{V}{I}\right) f_1 f_2$$

where

t is the thickness of the sample (cm),

V is the voltage measured (V),

I is the current through the sample (A) and

f_1 and f_2 are correction factors; here they are 1, because the probes are aligned in perfect symmetry.

In resistivity measurements a commercial anode was used as a reference: 4 mg cm^{-2} platinum ruthenium black—carbon cloth electrode from the Fuel Cell Store.

The SEM/energy dispersive x-ray spectroscopy (EDS) study was carried out with a Zeiss Merlin FE-SEM coupled with a Thermo Scientific NSS 3 energy dispersive X-ray (EDX) spectrometer. The samples were placed on an aluminium stub with a carbon tape. SEM images were collected by a secondary electron detector (SE) and an in-lens detector (In-lens SE) using 2.0 keV electron energy. EDX analysis was used for elemental analysis of the uncoated samples with an accelerating voltage of 15 keV.

The stacks were characterized using an optical microscope (Nikon Eclipse LV100ND) to observe the opened holes and the catalyst layer, as well as to check the electrochemical performance of the stacks. They were tested using a Greenlight fuel cell station G20 with a Gamry 3000 potentiostat using a H_2/air configuration.

3. Results

3.1. Ink formulation

The optimal ink formulation was 2.5 wt% C-Pt-Ru with 10% Nafion solution resulting in 0.5% Nafion concentration. DAA was used as the solvent vehicle. Earlier studies by Hakola *et al* have shown that stable water-based anode inks can also be formulated, but due to the need for surfactants, they are not considered feasible [20]. Three ink formulations were made: ink 1 without binders, ink 2 with 1 wt% PVP as a binder to improve ink stability and printability, and ink 3 with 1 wt% KD-14 as a binder. All inks were mixed using the same procedure: dispensing for 10 minand sonication for 15 min. For inks 2 and 3, binder was added after sonication and stirred for 6 h. Afterwards, all the inks were filtered with 5 μm plastic filters. Measured viscosity and surface tension are presented in table 1.

All the inks had a surface tension of approximately 30 mN m^{-1} that is ideal for inkjet printing in the range of 24–36 mN m^{-1}. The viscosities of the inks are slightly smaller than ideal (8–20 cP), but not critically too low. Also all the inks showed Newtonian behavior, ideal for inkjets. The low viscosity was not expected to cause issues with printability, such as spontaneous dripping from the printhead, and no further efforts to increase the viscosities were carried out. The inks were stored at room temperature for several weeks, and no significant particle agglomeration or sedimentation was observed, thus indicating that stable formulations were achieved.

Table 1. Surface tension and viscosity of the formulated inks.

	Ink 1	Ink 2	Ink 3
Binder	—	PVP	KD-14
Surface tension	30 mN m^{-1}	30 mN m^{-1}	30.9 mN m^{-1}
Viscosity	5 cP (Newtonian)	5.36 cP (Newtonian)	5.87 cP (Newtonian)

During formulation it was observed that some of the particle sediment at the bottom of the containers and inthe filters, thus indicating that the final C–Pt–Ru concentration was lower than the targeted concentration. Far more precise observation particle size calculations were carried out to see if an increase in catalyst concentration really increased the post-filtering catalyst loading. Five inks that had a different C–Pt–Ru concentration without binder were formulated: 0.5–2.5 wt% at the intervals of 0.5. The results are presented in figure 5. It can be seen that the increase in catalyst concentration increases the amount of the smallest particles (<10 μm) in the ink, thus indicating that the catalyst concentration indeed increases when most of the largest particles (>5 μm) are filtered off.

To determine the actual C–Pt–Ru concentration in the ink the formulations were weighted before dispensing, after dispensing, after sonication and after filtering. The weights were used to calculate the loss of particles during the formulation process. The actual C–Pt–Ru concentration in the final inks with 2.5 wt% initial concentration was approximately 2 wt%. This loss in particles was taken into account when printing the anodes for a specific targeted catalyst concentration.

3.2. Anode printing

All inks were printed with the laboratory scale printheads on the paper substrate. The printing layout was 2 cm × 2 cm areas. In addition, ink 2 (the one with PVP) was printed with industrial scale printheads to evaluate its up-scalability potential (ink 2 industrial). With both printhead types, the waveform, drive voltage and firing frequency were optimized for the best drop formation. The jetting performance of both inks with both printhead types is presented in table 2. The target catalyst concentration for printing was 1.6 mg cm^{-2} meaning that multiple ink layers were printed with both printhead types calculated based on print resolution, drop size and catalyst concentration in ink. The resulting printed surfaces, including thickness profiles, are presented in table 2.

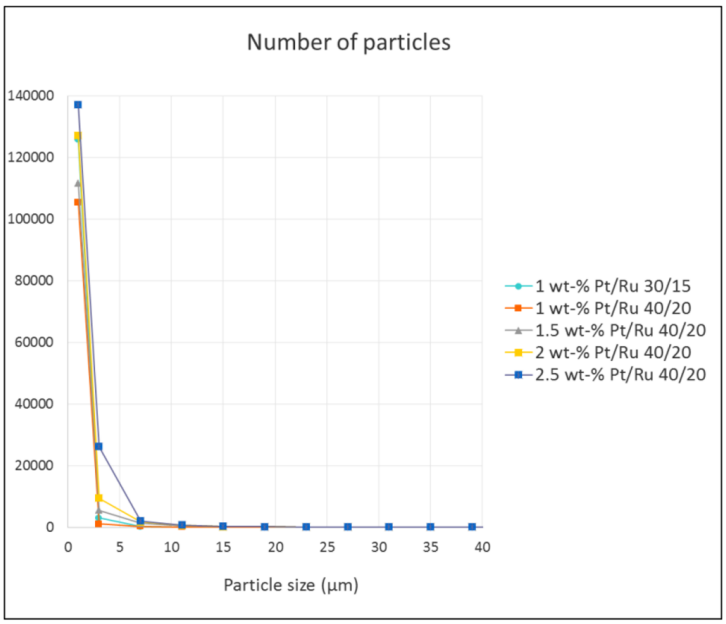

Figure 5. Particle size calculations with different C–Pt/Ru concentrations.

Table 2. Printability results for the different inks and printhead types. Drop formation describes how the drops come out of the printhead nozzles, and the goal is to have the drop tail disappear before the drops hit the surface of the substrate.

	Ink 1	Ink 2	Ink 2 industrial	Ink 3
Drop formation	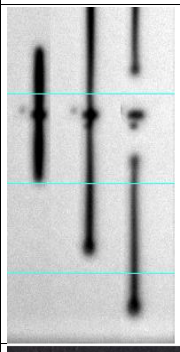	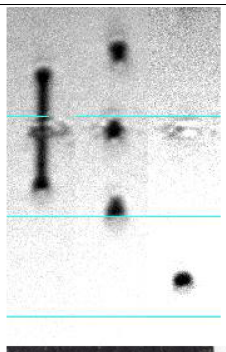		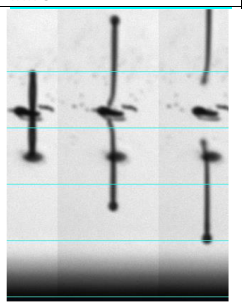
Area with mobile phone magnifying lens		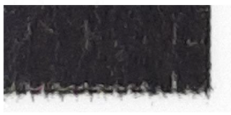		
Area taken with the camera integrated with the printer			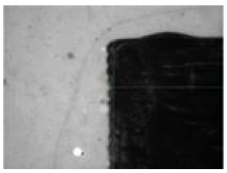	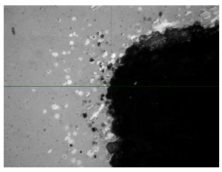
SEM with 10k magnification	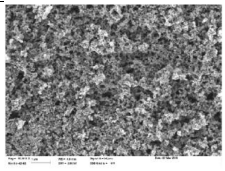	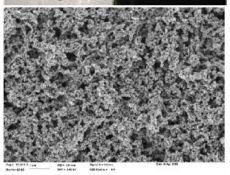	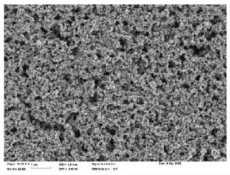	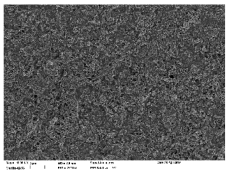
Thickness profile	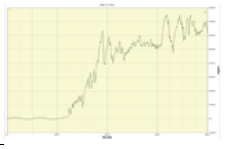		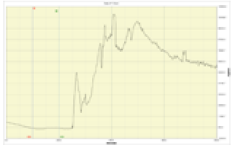	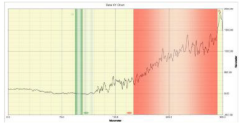

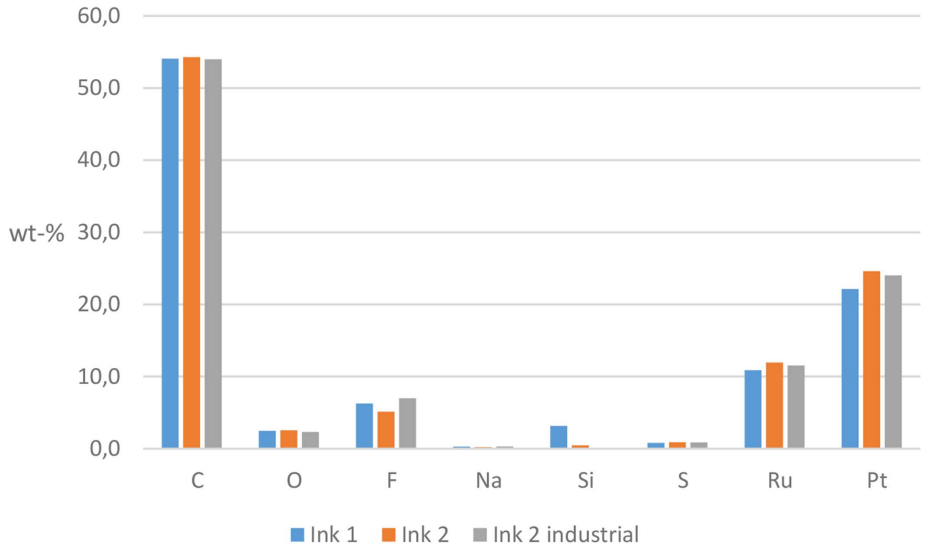

Figure 6. Elemental composition of the areas printed with the different inks.

All the inks show drop formation typical of inkjet printing, but drop formation looks better with inks that contain binder, because the ink tail completely disappears with ink 2 and is shorter with ink 3 than with ink 1. There are satellite drops or splashed drops at the edges of the printed areas when laboratory-scale printheads are used. This is probably more of a feature of the single-use laboratory-scale printheads than of the ink since there are no satellite drops present when printing with the more robust and high-quality industrial printhead. There is some non-uniformity in the layer when printed with the industrial-scale printhead. This is probably due to the use of a larger drop size resulting in more ink per one layer. This causes challenges in ink drying, thus causing defects in the layer's visual quality. Thickness profile measurements support this observation. With the industrial-scale printheads the thickness profile is not very uniform when compared with the profiles made with laboratory-scale printheads. The layer thicknesses were on average 3 μm (2 μm standard deviation for ink 1), 3 μm (1.5 μm standard deviation) for ink 2, 0.4 μm (0.3 μm standard deviation) for ink 3 and 6 μm (3.9 μm standard deviation) for ink 2 with industrial-scale printheads. The large difference between the thicknesses of ink 2 and ink 3 layers is probably a result of how different binders change how the ink interacts with the substrate. PVP (ink 2) might keep the ink particles stronger together and more agglomerates can be formed, while KD-14 (ink 3) could be weaker allowing the particles to spread more with the ink vehicle and into a thinner and more even layer. This observation is supported by profilometric images, where there are less thickness variations with ink 3, but also with the SEM images. The SEM images show that there are larger particle agglomerates when printed with ink 1 than with ink 2. This indicates that PVP keeps the particles better dispersed in the ink, thus affecting the layer quality. However, all printed areas have high porosity. This is beneficial for catalyst layers since a high surface area increases areas for electrochemical reactions. With ink 3 the layer looks more uniform than with ink 2, thus indicating that KD14 binder (ink 3) keeps the particles better dispersed than PVP (ink 2).

Resistivity measurements for the films gave similar values. For the ink without binder (ink 1) a value of 0.14 Ω cm was measured. For the ink with PVP (ink 2) when printed with the laboratory-scale printheads, the resistivity was 0.11 Ω cm (van der Pauw) and 0.12 Ω cm (linear). When the ink with PVP was printed with the industrial-scale printheads, the resistivity values with the two measurement methods were 0.19 Ω cm (van der Pauw) and 0.20 Ω cm (linear). When PVP is used in the ink the resistivity is slightly smaller. It might be that PVP as a binder keeps the particles more stable during printing and drying. Due to this the resulting layers have better uniformity affecting the resistivity, also seen in the thickness profile images (table 2) when comparing ink 1 and ink 2 with laboratory-scale printheads. With the industrial scale printheads the resistivity is slightly larger, probably due to the defects in the visual layer quality observed in the microscopic images (table 2). With ink 3 the resistivity values were difficult to calculate due to uncertainty in the thickness measurements. The resistivity values were approximately 0.1 Ω cm. The commercial anode electrode had a resistivity of 0.05 Ω cm. Although this value is smaller than with the printed anodes, it is, however, in the same range.

SEM/EDS analysis was used to analyse the catalyst content on the printed layers from inks 1 and 2. Figure 6 shows the elemental composition of the printed samples. Si comes from the paper substrate,

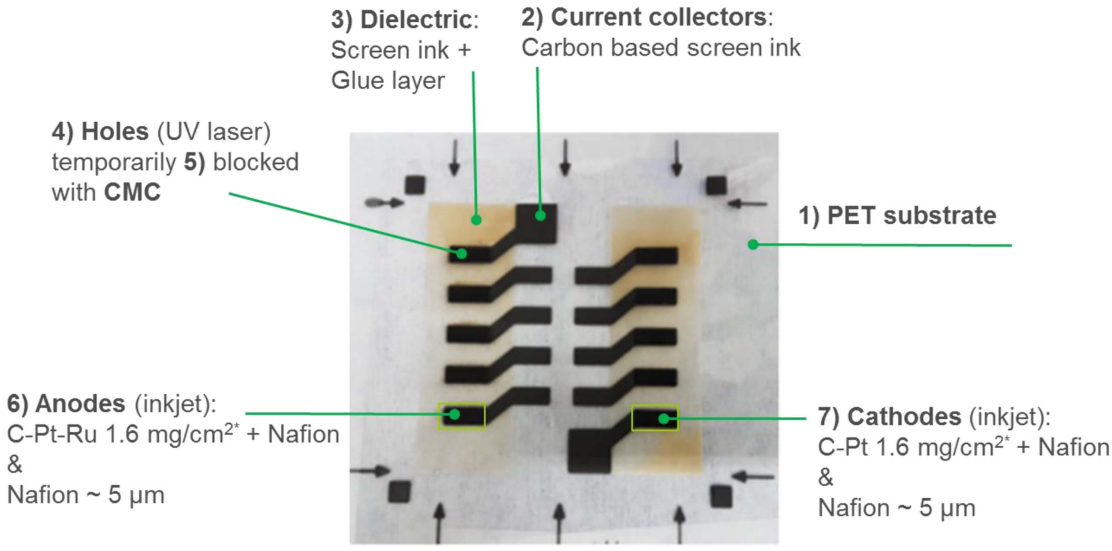

Figure 7. Different stack manufacturing steps in the order of 1–7 and the resulting stack before lamination.

and F, S and O from Nafion. The area printed with ink 2 has the largest concentration of both C, Pt and Ru corresponding to the lowest resistivity value. Ink 1 and ink 2 with industrial printheads have quite the same C concentration, but ink 1 has less Pt and Ru. This indicates that without PVP part of the catalyst particles probably sediment at the bottom of the ink reservoir during printing, thus not ending up on the substrate. A lower concentration of C, Pt and Ru, when printed with industrial scale printheads, is probably due to the non-uniform layer structure. The ratio between Pt and Ru on the printed layers is the same as with the original particle mixture, approximately 2:1. The ratio between C and PtRu is approximately 11:7 on printed areas. In the original ink the ratio is 2:3. Part of the C might be from the substrate, but its measured value might be inaccurate due to EDS's limited capability for low atomic number element identification causing uncertainty in the measured C composition. However, there should still be a sufficient amount of PtRu left on the printed layer, and the PtRu ratio is still the same as in the original composition.

3.3. Stack printing

Inks 2 and 3 were used to produce an anode for a fully printed passive fuel cell stack. This stack design may be operated in air-breathing mode with reactant flow only used on the anode side or in fully-passive fuel cell mode (without flow on both sides). The experiments were performed using the air-breathing configuration with H_2 as a fuel to limit the complexities associated with fuel crossover, which can deleteriously affect DMFCs. The manufacturing steps of the fuel cell stack are presented in figure 7. There are five anodes and five cathodes in the stack, and their size is 15 mm × 6 mm.

At first the current collectors were screen printed on the PET substrate with a carbon-based ink. A dielectric layer was screen printed around the current collectors, and a glue layer for lamination was screen printed on top of the dielectric layer. Holes through the PET substrate and current collectors were made with a UV laser with a hole diameter of approximately 400, 500 and 600 μm. The holes were temporarily blocked by screen printing a layer of CMC on the reverse side of the substrate. Anodes were inkjet printed with ink 2 or 3 on top of the current collectors with a catalyst loading of 1.6 mg_{PtRu} cm^{-2}. On top of the anodes a Nafion layer (8 wt% Nafion in DAA) was inkjet printed with a thickness of approximately 5 μm. Cathodes were inkjet printed with a similar formulation as ink 3, but C–Pt–Ru was replaced with C–Pt. The cathode catalyst loading was 1.6 mg_{Pt} cm^{-2}. The Nafionlayer was also inkjet printed on top of the cathodes to ensure that the Nafion layers provide good enough insulation between the anode and the cathode.

3.4. Stack characterization

For the electrochemical characterization the printed stack was assembled into an open cathode configuration; the stack parts were cut with scissors and after all the components were laminated (figure 8).

The assembly of the stack was carried out using a double-sided acrylic glue sticker (3 M 400 MP). Some resin reinforced with glass fiber (PCB base boards FR4) was used as flow channels for the anode part. When all the parts were assembled, the stack was hot-pressed at 60 kg cm^{-2} at 140 °C for 5 min to improve the contact with the Nafion and the catalyst layer. Next, the temperature was decreased to 70 °C and held for 1 h to cure the glue. As shown in figure 8(c), a layer of Nafion® 212 (50.8 μm) was added to avoid any possible short circuit in the stack. Some optical

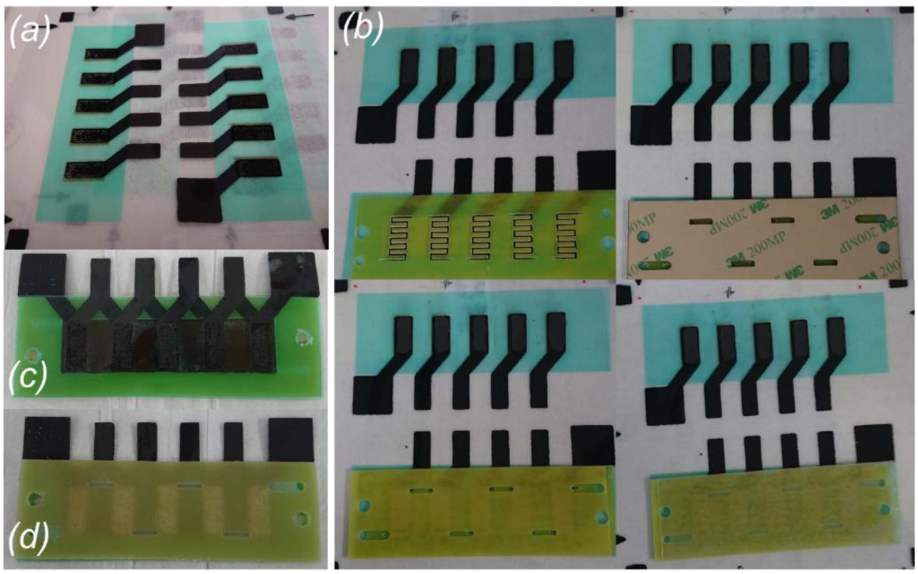

Figure 8. (a) A view of the anode and cathode catalyst layers (inside). (b) Lamination steps for the printed stack, (c) and (d) the final stack assembled cathode and anode side, respectively (air-breathing configuration).

images of the layers were taken over the stacks to observe the front and backside (figure 9).

In the front side (figure 9(a)) image, it is possible to observe a green region related to the isolation material to avoid a short circuit between the single cells. On top of the catalyst layer a type of plastic surface can be observed due to the Nafion layer inkjet printing and some fully opened holes when the blocking CMC layer was removed with water. In figure 9(b) the back part of the anode side is shown; on this side the covered holes show the carbon current collector and gas diffusion layer.

The stacks were tested under H_2/air configuration (air-breathing mode) to check if there was any issue in the device assembly, due to the fast reaction of H_2 over the Pt catalyst; this means that if no open circuit potential (OCP) is measured the stack has a short circuit due to assembly problems.

Figure 10 shows the five-cell stack performance for ink 2 (PVP as a binder) under H_2/air conditions; a value of 3.4 V (0.680 V each cell) of OCP was obtained, lower than expected for a H_2 fuel cell stack (should be around 4.5 V, 0.9 V each). The peak power of this stack was 120 μW cm^{-2} at 1.75 V, with a resistance obtained from the potentiostatic impedance of 295 Ohm cm^2.

The second stack assembled using ink 3 (KD-14 as the binder) shows a poorer performance (figure 11) under H_2/air conditions; a value of 2.43 V of OCP was obtained with a peak power of 100 μW at 0.5 V, for this stack, and the resistance was 11.16 Ohm cm^2. The results indicate that when using PVP as a binder, the fuel cell stack has better performance.

The manufactured stacks were not dense enough to be tested with methanol due to the need for an additional Nafion film. Another limiting factor was that some of the holes on the current collector were not blocked by anode or cathode material due to failures during the CMC layer removal process. This created too much leakage during methanol testing, and no reliable results were obtained.

4. Discussion

A novel approach for catalyst ink formulation and for the manufacture of a fully printed fuel cell stack have been reported in this paper. Catalyst ink formulation for inkjet printing requires consideration of ink rheology (selection of solvent, surface tension, viscosity) and ink stability during storage and printing (avoidance of particle agglomeration and sedimentation). Towne *et al* have formulated a stable water-based ink based on a Pt/C catalyst and Nafion solution for use as an MEA in a hydrogen-air PEMFC with catalyst loading of 0.20 mg cm^{-2} [21]. In that paper, printing was carried out with off-the-shelf office printers. They achieved a similar performance compared to commercial MEAs (OCP 0.87 V, peak power 155 mW cm^{-2}), but all the parts of the stack were not printed in contrast to the research presented in this paper. The stack assembly process can have a great effect on fuel cell performance. Thereby, their results are not fully comparable with the results achieved here with a fully printed stack. Another difference is the main solvent used in the catalyst ink. The use of water as a main solvent has the potential to cause issues due to the need for surfactants in order to decrease the surface tension of the ink to a proper level. Even non-ionic surfactants have the potential to interfere with the electrochemical performance of the electrodes, and thus their use should be avoided [20]. Also Taylor *et al* have evaluated inkjet printable

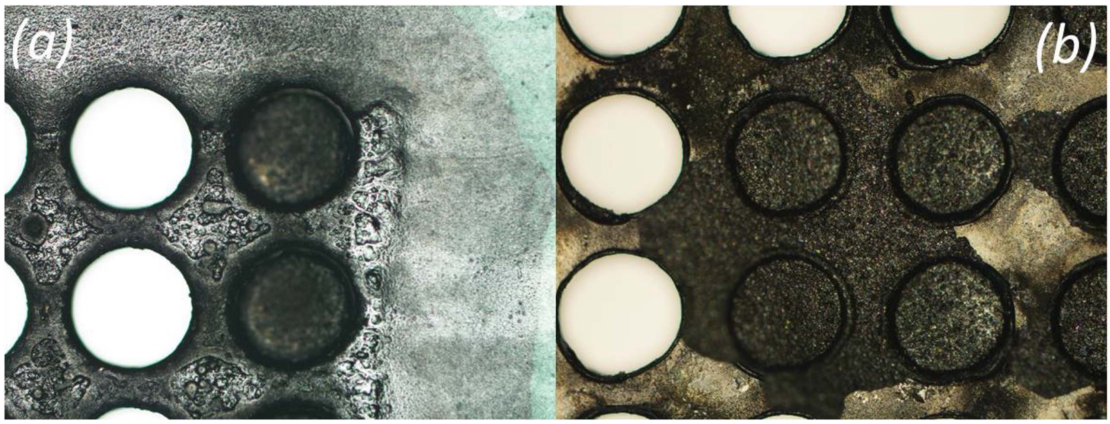

Figure 9. (a) Front and (b) back images of the anode side in the single cell.

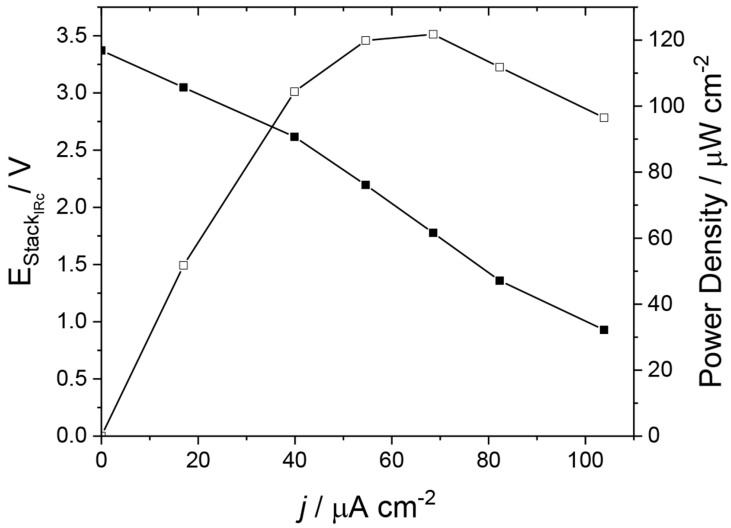

Figure 10. A polarization curve of the stack assembled with ink 2 (PVP as binder), with a H_2 flow of 50 ml min^{-1} in the anode and air-breathing in the cathode at 21 °C using the Nafion 212 layer and 1 cm^2 area of each cell.

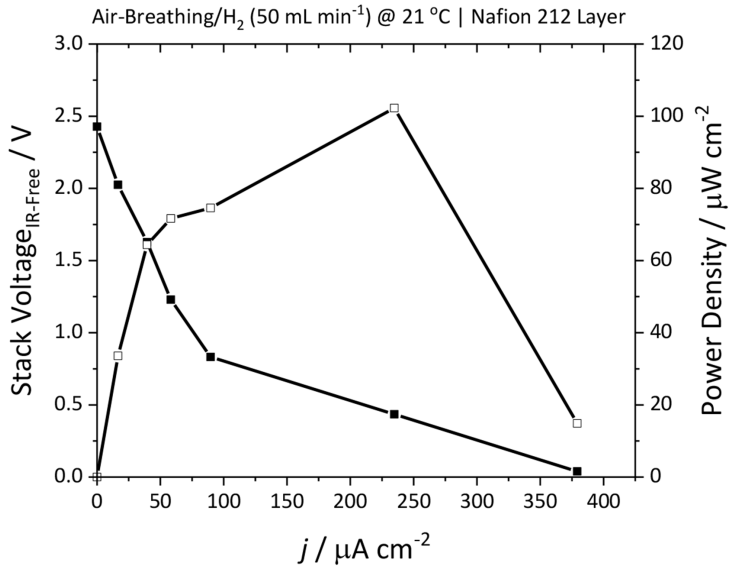

Figure 11. A polarization curve of the stack assembled with ink 3 (KD-14 as binder), with a H_2 flow of 50 ml min^{-1} in the anode and air-breathing in the cathode at 21 °C using the Nafion 212 layer and 1 cm^2 area of each cell.

MEAs for PEMFC fabrication based on a Pt/C catalyst with 0.020 mg cm^{-2} catalyst loading [18]. They used methanol as the main ink solvent for a catalyst ink printable with an office printer. Flexible fuel cell devices have also been developed based on polymeric materials, but these do not use only printing processes in the manufacturing flow [22–24].

The main challenges causing insufficient stack performance in this paper with both the stack voltage (3.4 V achieved with 4.5 V target) and compatibility with methanol fuel arose from the stack assembly process after electrode printing. This caused the stacks to not be dense enough to act as DMFCs and decreased the stack performance. Modification of the CMC ink formulation might have an effect on this by minimizing the CMC concentration. Another challenge was with the Nafion layer used as the membrane between the electrodes. Although an inkjet printable Nafion ink was formulated and successfully printed, it most probably did not provide full electrical insulation between the electrodes, leading to an internal short circuit and necessitating the inclusion of an additional Nafion film during stack assembly. However, the printed anodes showed almost similar resistivity to commercially available electrodes, 0.1 Ω cm and 0.05 Ω cm respectively, when characterized in single-cell fuel cell test rigs. In a recent conference paper [25] published by some of the authors of this paper, the inkjet-printed anodes have successfully performed as part of a single cell DMFC. Thereby, it can be concluded that the inkjet printed electrode works, but the fully printed stack still needs refining in the different fuel-cell parts to obtain a fully functional fuel cell with the capability to use H_2 and methanol.

5. Conclusions

This paper shows that it is possible to manufacture fully printed flexible and thin passive H_2 fuel cell stacks, although targeted stack performance using methanol was not obtained. Further improvements in the catalyst layer printing and of the stack manufacturing process could potentially also improve the stack performance and stability. One of the main challenges observed was the CMC layer removal also resulting, many times, in removal of the anode and the cathode layer. However, the printed electrodes show a performance suitable for energy requirement solutions, such as powering up single-use sensors. Specifically, it is possible to use inkjet printable electrodes, and stable formulations have been achieved. The printed anodes show almost similar resistivity to commercially available electrodes.

One application for the demonstrated fuel cell stacks could be to use them as a part of an autonomous electrochemical biosensor, where the bioreceptor element is hosted inside a passive fuel cell [25, 26]. In the envisaged device, the electrical signal obtained from the fuel cell is directly related to the concentration of the cancer biomarker in the sample analysed.

Acknowledgments

The work reported in this paper has received funding from the European Commission under the framework of the Horizon 2020 Symbiotic project (Grant Agreement No. 665056). Project partners are acknowledged for their collaboration. Parts of the facilities used were provided by the Academy of Finland Research Infrastructure, the Printed Intelligence Infrastructure (PII-FIRI, Grant No. 32020).

The authors would like to offer special thanks to Senior Research Technician Pirjo Hakkarainen for her dedicated laboratory work. Also Senior Scientist Asko Sneck is acknowledged for carrying out SEM/EDS analysis.

ORCID iDs

Liisa Hakola https://orcid.org/0000-0002-8394-6277
Andres Parra Puerto https://orcid.org/0000-0002-1131-1168
Anthony Kucernak https://orcid.org/0000-0002-5790-9683

References

[1] Lesch A, Cortés-Salazar F, Bassetto V C, Amstuzt V and Girault H H 2015 Inkjet printing meets electrochemical energy conversion *Chimia* **69** 284–9
[2] Jenkins P, Tuurala S, Vaari A, Valkiainen M, Smolander M and Leech D 2012 A mediated glucose/oxygen enzymatic fuel cell based on printed carbon inks containing aldose dehydrogenase and laccase as anode and cathode *Enzyme Microb. Technol.* **50** 181–7
[3] Hast J, Jansson E, Suhonen R, Hakola L, Tuomikoski M, Vilkman M, Rönkä K and Kopola H 2017 Printed electronics solutions-based processes with flexible glass *Flexible Glass: Enabling Thin, Lightweight and Flexible Electronics* ed S M Garner (Beverly, MA: Scrivener) pp 181–210
[4] Kipphan H 2001 *Handbook of Print Media* (Berlin: Springer) p 1207
[5] Zalitis C M, Kucernak A R, Sharman J and Wright E 2017 Design principles for platinum nanoparticles catalysing electrochemical hydrogen evolution and oxidation reactions: edges are much more active than facets *J. Mater. Chem.* A **5** 23328–38
[6] Kucernak A R and Zalitis C 2016 General models for the electrochemical hydrogen oxidation and hydrogen evolution reactions: theoretical derivation and experimental results under near mass-transport free conditions *J. Phys. Chem.* C **120** 10721–45
[7] Deiner L J and Reitz T L 2017 Inkjet and aerosol jet printing of electrochemical devices for energy conversion and storage *Adv. Eng. Mater.* **19** 18
[8] Koiramäki V 2016 Development of printable membrane electrode assembly for a passive direct methanol fuel cell-based biosensor *Bachelor's Thesis* Metropolia Ammattikorkeakoulu p 58
[9] Koraishy B M, Solomon S, Meyers J P and Wood K L 2012 Parametric investigations of direct methanol fuel cell

electrodes manufactured by spraying *J. Fuel Cell Sci. Technol.* **9** 5
[10] US Department of Energy 2001 *Hydrogen Fuel Cell Engines Module 1: Hydrogen Properties Contents* (Palm Desert, CA: College of the Desert) p 47
[11] Soloveichik G L and Nanotechnol B J 2014 Liquid fuel cells **5** 1399–418
[12] Chen X, Li T, Shen J and Hu Z 2017 From structures, packaging to application: a system-level review for micro direct methanol fuel cell *Renew. Sustain. Energy Rev.* **80** 669–78
[13] Wang L, He M, Hu Y, Zhang Y, Liu X and Wang G 2015 A "4-cell" modular passive DMFC (direct methanol fuel cell) stack for portable applications *Energy* **82** 229–35
[14] Joghee P, Malik J N, Pylypenko S and O'Hayre R 2015 A review on direct methanol fuel cells—in the perspective of energy and sustainability *MRS Energy Sustainability* **4** 1–31
[15] Zheng W, Suominen A and Tuominen A 2012 Discussion on the challenges of DMFC catalyst loading process for mass production *Energy Procedia* **28** 78–87
[16] Liu H, Song C, Zhang L, Zhang J, Wang H and Wilkinson D P 2006 A review of anode catalysis in the direct methanol fuel cell *J. Power Sources* **155** 95–110
[17] Zhou W J, Zhou B, Li W Z, Zhou Z H, Song S Q, Sun G Q, Xin Q, Douvartzides S, Goula M and Tsiakaras P 2004 Performance comparison of low-temperature direct alcohol fuel cells with different anode catalysts *Power Sources* **126** 16–22
[18] Taylor A D, Kim E Y, Humes V P, Kizuka J and Thompson L T 2007 Inkjet printing of carbon supported platinum 3-D catalyst layers for use in fuel cells *J. Power Sources* **171** 101–6
[19] Keithley Application Note 2011 *Four-Probe Resistivity and Hall Voltage Measurements with the Model 4200-SCS* (Solon, OH: Keithley Instruments) p 8
[20] Hakola L, Maaninen T, Tuurala S and Vaari A 2016 Inkjet printable anode ink for fuel cell applications *Proc. of Printing for Fabrication 2016 Conf., the 32nd Int. Conf. on Digital Printing Technologies (NIP) (Manchester, UK)* pp 149–52
[21] Towne S, Viswanathan V, Holbery J and Rieke P 2007 Fabrication of polymer electrolyte membrane fuel cell MEAs utilizing inkjet print technology *J. Power Sources* **171** 575–84
[22] Wu Z, Kuang X, Liu L and Wang X 2017 A flexible foldable tubular μDMFC for powering wearable devices *J. Microelectromech. Syst.* **26** 1147–54
[23] Weinmueller C, Tautschnig G, Hotz N and Poulikako D 2010 A flexible direct methanol micro-fuel cell based on a metalized, photosensitive polymer film *J. Power Sources* **195** 3849–57
[24] Ito T, Kimura K and Kunimatsu M 2006 Characteristics of micro DMFCs array fabricated on flexible polymeric substrate *Electrochem. Commun.* **8** 973–6
[25] Parra Puerto A, Hakola L and Kucernak A R J 2018 Low cost PCB fuel cells based for small electronic applications *Proc. 233rd ECS Meeting (Seattle, USA)*
[26] Sales M G F and Lúcia Brandão L 2017 Autonomous electrochemical biosensors: a new vision to direct methanol fuel cells *Biosens. Bioelectron.* **98** 428–36